The Astrophysical Journal, 715:458–467, 2010 May 20 doi:10.1088/0004-637X/715/1/458

HAT-P-14b: A 2.2 M_J EXOPLANET TRANSITING A BRIGHT F STAR*

G. Torres[1], G. Á. Bakos[1,10], J. Hartman[1], Géza Kovács[2], R. W. Noyes[1], D. W. Latham[1], D. A. Fischer[3], J. A. Johnson[4,11], G. W. Marcy[5], A. W. Howard[5], D. D. Sasselov[1], D. Kipping[1,6], B. Sipőcz[1,7], R. P. Stefanik[1], G. A. Esquerdo[1], M. E. Everett[8], J. Lázár[9], I. Papp[9], and P. Sári[9]

[1] Harvard-Smithsonian Center for Astrophysics, Cambridge, MA, USA; gtorres@cfa.harvard.edu
[2] Konkoly Observatory, Budapest, Hungary
[3] Department of Physics and Astronomy, San Francisco State University, San Francisco, CA, USA
[4] Institute for Astronomy, University of Hawaii, Honolulu, HI, USA
[5] Department of Astronomy, University of California, Berkeley, CA, USA
[6] Department of Physics and Astronomy, University College London, UK
[7] Centre for Astrophysics Research, University of Hertfordshire, Hatfield, UK
[8] Planetary Science Institute, Tucson, AZ, USA
[9] Hungarian Astronomical Association, Budapest, Hungary
Received 2010 February 11; accepted 2010 March 30; published 2010 April 29

ABSTRACT

We report the discovery of HAT-P-14b, a fairly massive transiting extrasolar planet orbiting the moderately bright star GSC 3086-00152 ($V = 9.98$), with a period of $P = 4.627669 \pm 0.000005$ days. The transit is close to grazing (impact parameter $0.891^{+0.007}_{-0.008}$) and has a duration of 0.0912 ± 0.0017 days, with a reference epoch of mid-transit of $T_c = 2{,}454{,}875.28938 \pm 0.00047$ (BJD). The orbit is slightly eccentric ($e = 0.107 \pm 0.013$), and the orientation is such that occultations are unlikely to occur. The host star is a slightly evolved mid-F dwarf with a mass of $1.386 \pm 0.045\ M_\odot$, a radius of $1.468 \pm 0.054\ R_\odot$, effective temperature 6600 ± 90 K, and a slightly metal-rich composition corresponding to [Fe/H] $= +0.11 \pm 0.08$. The planet has a mass of $2.232 \pm 0.059\ M_J$ and a radius of $1.150 \pm 0.052\ R_J$, implying a mean density of 1.82 ± 0.24 g cm^{-3}. Its radius is well reproduced by theoretical models for the 1.3 Gyr age of the system if the planet has a heavy-element fraction of about 50 $M_\oplus$ (7% of its total mass). The brightness, near-grazing orientation, and other properties of HAT-P-14 make it a favorable transiting system to look for changes in the orbital elements or transit timing variations induced by a possible second planet, and also to place meaningful constraints on the presence of sub-Earth mass or Earth-mass exomoons, by monitoring it for transit duration variations.

Key words: planetary systems – stars: individual (HAT-P-14, GSC 3086-00152) – techniques: photometric – techniques: spectroscopic

Online-only material: machine-readable table

1. INTRODUCTION

More than five dozen transiting extrasolar planets (TEPs) have been discovered to date, by both ground-based surveys and, recently, space-based surveys such as the *CoRoT* and *Kepler* missions (Baglin et al. 2006; Borucki et al. 2010). The ground-based surveys are typically able to detect TEPs orbiting only the brighter stars. However, this disadvantage has the compensatory advantage that those TEPs detected are amenable to a wide range of follow-up studies, which can provide valuable insight into their atmospheric properties and other physical conditions.

Among the ground-based surveys, the Hungarian-made Automated Telescope Network (HATNet; Bakos et al. 2004) survey has been one of the main contributors to the discovery of TEPs. In operation since 2003, it has now covered approximately 11% of the sky, searching for TEPs around bright stars ($8 \lesssim I \lesssim 12.5$). HATNet operates six wide-field instruments: four at the Fred Lawrence Whipple Observatory (FLWO) in Arizona, and two on the roof of the hangar servicing the Smithsonian Astrophysical Observatory's Submillimeter Array, in Hawaii. Since 2006, HATNet has announced and published 13 TEPs. In this work we report our fourteenth discovery, around the relatively bright ($V = 9.98$) star we refer to as HAT-P-14, also known as GSC 3086-00152.

The layout of the paper is as follows. In Section 2, we report the detection of the photometric signal and the follow-up spectroscopic and photometric observations of HAT-P-14. In Section 3, we examine the spectroscopic evidence to confirm the planetary nature of the object. Section 4 describes the analysis of the data, beginning with the determination of the stellar parameters, and continuing with a description of our global modeling of the photometry and radial velocities (RVs). Results are presented in Section 5 and discussed in Section 6.

2. OBSERVATIONS

2.1. Photometric Detection

The transits of HAT-P-14b were detected with the HAT-10 telescope located in Arizona. Observations in a field containing the star GSC 3086-00152 were made on a nightly basis between 2005 May and July, as permitted by weather conditions. We gathered 1246 exposures of 150 s with a cadence of 3.2 minutes, 206 exposures of 180 s at 3.7 minute cadence, and 1991 exposures of 300 s at a 5.7 minute cadence. The reason for the somewhat inhomogeneous data set is that the observations were acquired during the commissioning phase of HAT-10. The first exposures with 150 s cadence were taken with an

* Based in part on observations obtained at the W. M. Keck Observatory, which is operated by the University of California and the California Institute of Technology.
[10] NSF Fellow.
[11] NSF Postdoctoral Fellow.

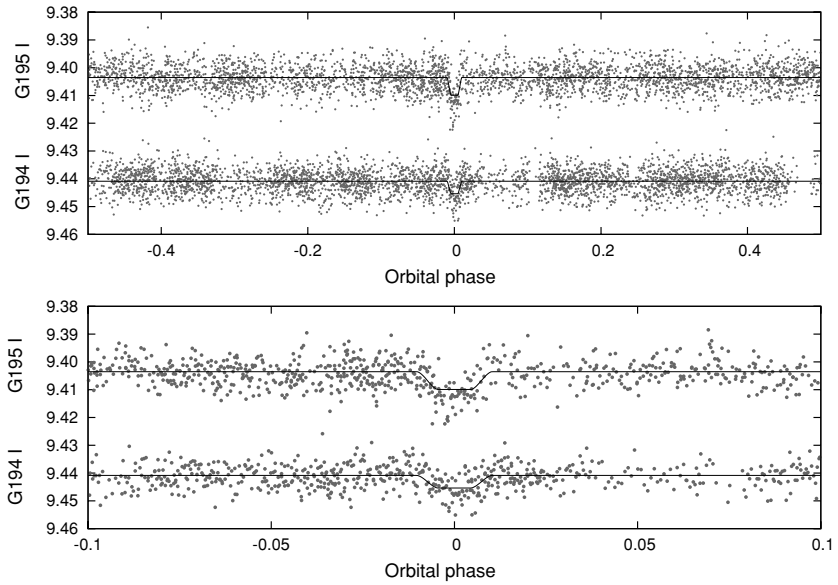

Figure 1. Top: unbinned *I*-band light curves of HAT-P-14 obtained with the HAT-5 and HAT-10 nodes of HATNet, showing all 3189 and 3443 instrumental measurements from fields G195 and G194, respectively. The photometry is phase-folded with the period $P = 4.627669$ days resulting from the global fit described in Section 4. The solid lines show the transit model fit to the light curves (Section 4.2). Bottom: the same, for phases within 0.1 of the transit center.

Apogee ALTA E42 back-illuminated CCD through a Cousins *I*-band filter. Exposure times were increased to 180 s after some initial testing. Finally, the CCD was replaced with an Apogee E10 front-illuminated model, and exposure times were further increased to 300 s. Each image contained approximately 22,000 stars down to a brightness limit of $I \sim 14.0$. For the brightest stars in the field we achieved a photometric precision of 3.5 mmag per image in the combined light curve.

The calibration of the HATNet frames was carried out using standard photometric procedures. The calibrated images were then subjected to star detection and an astrometric solution, as described in more detail by Pál & Bakos (2006). Aperture photometry was performed on each image at the stellar centroids derived from the Two Micron All Sky Survey (2MASS; Skrutskie et al. 2006) catalog and the individual astrometric solutions. The resulting light curves were decorrelated (cleaned of trends) using the External Parameter Decorrelation (EPD; see Bakos et al. 2010) technique in "constant" mode and the Trend Filtering Algorithm (TFA; see Kovács et al. 2005). The light curves were then searched for periodic box-shaped signals using the Box Least-Squares (BLS; Kovács et al. 2002) method. We detected a significant signal in the light curve of GSC 3086-00152 (also known as 2MASS 17202788+3814317; $\alpha = 17^{\rm h}20^{\rm m}27\overset{\rm s}{.}96$, $\delta = +38^\circ 14' 31\overset{''}{.}8$; J2000; $V = 9.98$; Droege et al. 2006), with an apparent depth of 4.5 mmag, and a period of $P = 4.6277$ days (see Figure 1). The drop in brightness had a first-to-last-contact duration q, relative the total period P, of $q = 0.0197 \pm 0.0004$, corresponding to a total duration of $Pq = 2.189 \pm 0.040$ hr.

HAT-P-14 falls in an overlapping area between two HATNet fields internally labeled G194 and G195. While the discovery was made on the basis of the G194 light curve, the signal was later recovered in the 3189 *I*-band observations from field G195. These latter data were taken during the commissioning phase of the HAT-5 telescope at FLWO, in early 2003, making this one of the TEPs with the longest photometric coverage. Curiously, the signal is present in the early HAT-5 (G195) data with higher significance than in field G194. The discovery of HAT-P-14 in 2003 was probably missed due to a combination of factors, including our different criteria for scheduling follow-up observations at the time, and the lack of the TFA, which was only implemented and brought into regular use in 2005.

2.2. Reconnaissance Spectroscopy

As is routine in the HATNet project, all candidates are subjected to careful scrutiny before investing valuable time on large telescopes. This includes spectroscopic observations at relatively modest facilities to establish whether the transit-like feature in the light curve of a candidate might be due to astrophysical phenomena other than a planet transiting a star. Many of these false positives are associated with large RV variations in the star (tens of km s^{-1}) that are easily recognized. For this we have made use here of the Harvard-Smithsonian Center for Astrophysics (CfA) Digital Speedometer (DS; Latham 1992), an echelle spectrograph mounted on the FLWO 1.5 m telescope. This instrument delivers high-resolution spectra ($\lambda/\Delta\lambda \approx 35{,}000$) over a single order centered on the Mg I b triplet ($\sim$5187 Å), with typically low signal-to-noise ratios (S/Ns) that are nevertheless sufficient to derive RVs with moderate precisions of 0.5–1.0 km s^{-1} for slowly rotating stars. The same spectra can be used to estimate the effective temperature, surface gravity, and projected rotational velocity of the host star, as described by Torres et al. (2002). With this facility we are able to reject many types of false positives, such as F dwarfs orbited by M dwarfs, grazing eclipsing binaries, or triple or quadruple star systems. Additional tests are performed with other spectroscopic material described in the next section.

For HAT-P-14 we obtained four observations with the DS between April and May of 2008. The velocity measurements showed an rms residual of 0.28 km s^{-1}, consistent with no detectable RV variation within the precision of the measurements. All spectra were single-lined, i.e., there is no evidence for additional stars in the system. The atmospheric parameters we infer from these observations are the following: effective temperature $T_{\rm eff\star} = 6500 \pm 100$ K, surface gravity $\log g_\star = 3.5 \pm 0.25$ (log cgs), and projected rotational velocity $v \sin i = 11.7 \pm 1.0$ km s^{-1}. The effective temperature

Table 1
Relative Radial Velocities, Bisector Spans, and Activity Index Measurements of HAT-P-14

BJD (2,454,000+)	RV[a] ($m\,s^{-1}$)	σ_{RV}[b] ($m\,s^{-1}$)	BS ($m\,s^{-1}$)	σ_{BS} ($m\,s^{-1}$)	S[c]
602.85803	−193.02	3.63	−5.39	6.36	0.469
602.86212[d]	...	...	−0.39	5.33	0.469
603.10266	−208.31	2.97	−0.62	5.69	0.471
603.86301	−163.07	3.39	−0.31	5.59	0.464
604.09553	−95.63	3.35	−8.06	6.65	0.461
633.99341	197.89	3.59	6.31	3.95	0.461
634.93450	−104.57	3.08	6.21	4.03	0.463
635.98053	−207.08	3.48	2.08	4.76	0.463
637.96376	200.73	3.10	1.88	4.99	0.464
639.01426	90.31	3.34	6.15	3.97	0.470
641.98653	101.38	4.20	1.57	4.96	0.459
777.70610	124.49	3.94	−0.40	5.36	0.459
955.08247	−213.27	3.65	−1.55	5.37	0.463
1017.01279	126.95	3.44	10.95	3.44	0.468
1106.77226	−27.59	4.34	−18.36	8.23	0.456

Notes.
[a] The zero point of these velocities is arbitrary. An overall offset γ_{rel} fitted to these velocities in Section 4.2 has *not* been subtracted.
[b] Internal errors excluding the component of astrophysical jitter considered in Section 5.
[c] Relative chromospheric activity index, not calibrated to the scale of Vaughan et al. (1978).
[d] This observation corresponds to the iodine-free template, which does not yield an RV measurement but does permit the BS and S index to be computed.

corresponds to a mid-F dwarf. The mean heliocentric RV of HAT-P-14 is $\gamma_{RV} = -20.81 \pm 0.28\ km\,s^{-1}$.

2.3. High-resolution, High-S/N Spectroscopy

Given the statistically significant transit detection by HATNet, and the encouraging DS results that rule out obvious false positives, we proceeded with the follow-up of this candidate by obtaining high-resolution, high-S/N spectra in order to characterize the RV variations with higher precision, and to refine the determination of the stellar parameters. For this we used the HIRES instrument (Vogt et al. 1994) on the Keck I telescope located on Mauna Kea, Hawaii, between 2008 May 15 and 2009 October 1. The width of the spectrometer slit was 0.″86, resulting in a resolving power of $\lambda/\Delta\lambda \approx 55{,}000$, with a wavelength coverage of ∼3800–8000 Å.

We obtained a total of 14 exposures through an iodine gas absorption cell, which was used to superimpose a dense forest of I_2 lines on the stellar spectrum and establish an accurate wavelength fiducial (see Marcy & Butler 1992). An additional exposure was taken without the iodine cell, for use as a template in the reductions. Relative RVs in the solar system barycentric frame were derived as described by Butler et al. (1996), incorporating full modeling of the spatial and temporal variations of the instrumental profile. The RV measurements and their uncertainties are listed in Table 1. The period-folded data, along with our best fit described below in Section 4, are displayed in Figure 2.

In the same figure we show also the relative S index, which is a measure of the chromospheric activity of the star derived from the flux in the cores of the Ca II H and K lines. This index was computed following the prescription given by Vaughan et al. (1978), after matching each spectrum to a reference spectrum using a transformation that includes a wavelength shift and a flux scaling that is a polynomial as a function of wavelength.

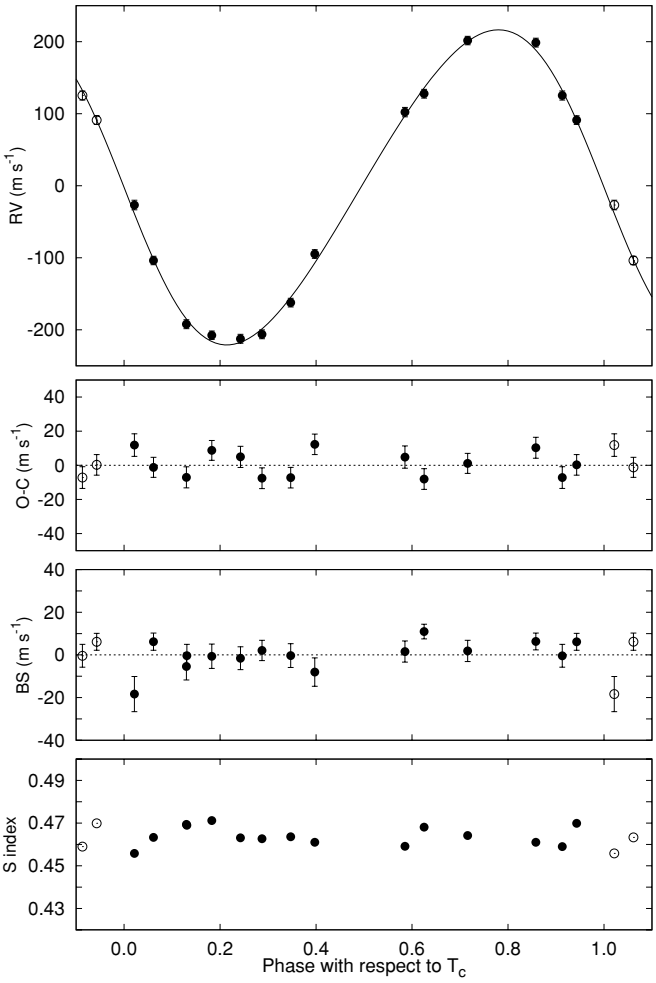

Figure 2. Top panel: Keck/HIRES RV measurements for HAT-P-14 shown as a function of orbital phase, along with our best-fit model (see Table 4). Zero phase corresponds to the time of mid-transit. The center-of-mass velocity has been subtracted. Second panel: velocity $O - C$ residuals from the best fit. The error bars (which are too small to be seen in the top panel) include a component from astrophysical jitter ($7.3\ m\,s^{-1}$) added in quadrature to the formal errors (see Section 5). Third panel: bisector spans (BS), with the mean value subtracted. The measurement from the template spectrum is included. Bottom panel: relative chromospheric activity index S measured from the Keck spectra. Note the different vertical scales of the panels. Observations shown twice are represented with open symbols.

The transformation was determined on regions of the spectra that are not used in computing this indicator. Note that our relative S index has not been calibrated to the scale of Vaughan et al. (1978). We do not detect any significant variation of the index correlated with orbital phase; such a correlation might have indicated that the RV variations could be due to stellar activity, casting doubt on the planetary nature of the candidate. There is no sign of emission in the cores of the Ca II H and K lines in any of our spectra, from which we conclude that the chromospheric activity level in HAT-P-14 is very low.

2.4. Photometric Follow-up Observations

In order to permit a more accurate modeling of the light curve, we conducted additional photometric observations with the KeplerCam CCD camera on the FLWO 1.2 m telescope. We observed five transit events of HAT-P-14 on the nights of 2008 October 19, 2009 February 2, 2009 March 25, 2009 April 8, and 2009 May 15 (Figure 3). A Sloan i-band filter was used for

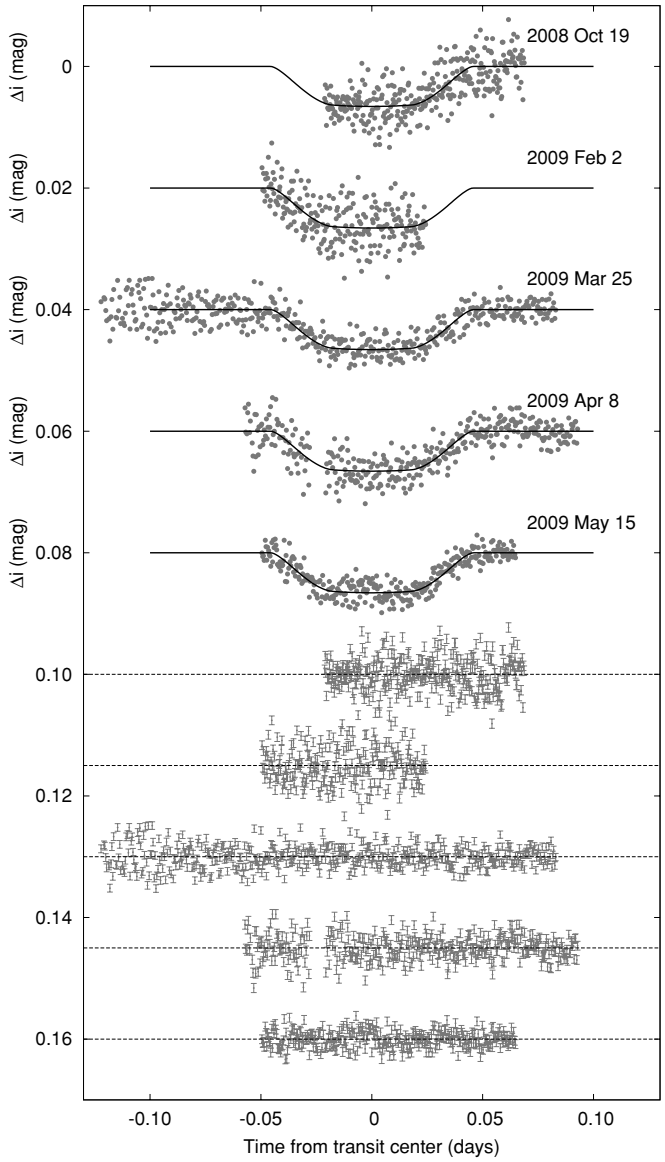

Figure 3. Unbinned instrumental transit light curves in the Sloan *i* band, acquired with KeplerCam on the FLWO 1.2 m telescope. The light curves have been processed with EPD and TFA, as described in Section 4.2. The dates of the events are indicated. Curves after the first are displaced vertically for clarity. Our best fit from the global modeling described in Section 4.2 is shown by the solid lines. Residuals from the fits are displayed at the bottom, in the same order as the top curves. The error bars represent the photon and background shot noise, plus the readout noise.

all observations. The number of images we acquired on each of these events is 326, 239, 470, 359, and 304, respectively. The exposure times were 10, 13, 20, 15, and 15 s, resulting in a cadence of 22, 25, 32, 27, and 27 s. The reduction of these images, including basic calibration, astrometry, aperture photometry, and trend removal, was performed as described by Bakos et al. (2010). The final time series are shown in the top portion of Figure 3, along with our best-fit transit light curve model described below; the individual measurements are reported in Table 2.

3. FALSE POSITIVE REJECTION

Our initial spectroscopic analyses discussed in Section 2.2 and Section 2.3 rule out the most obvious astrophysical false positive scenarios. However, more subtle phenomena such as blends (contamination by an unresolved eclipsing binary, whether in the background or associated with the target) can still mimic both the photometric and spectroscopic signatures we see. Following Torres et al. (2007), we explore here the possibility that the measured Keck/HIRES RVs are not real, but are instead caused by distortions in the spectral line profiles due to this contamination. We determined the spectral line bisectors and corresponding bisector spans (a measure of the line asymmetry) from each of our Keck spectra as described in Section 5 of Bakos et al. (2007). The bisector spans are displayed in the third panel of Figure 2. At first glance there is little variation as a function of orbital phase, in contrast to the $\sim$400 m s^{-1} peak-to-peak change in the RVs shown in the top panel. However, closer examination gives the visual impression of a slight correlation with the RVs, in the sense that the bisector spans for the first half of the orbit tend to be zero or negative (as are the RVs), whereas those in the second half tend to be zero or positive (again following the RVs).

A Spearman rank-order correlation test indicates that a correlation as strong as that suggested between the bisector spans and the RVs would occur by chance 9.5% of the time (false-alarm probability (FAP)), which we do not consider to be small enough to confirm the apparent correlation at a significant level. If we remove one outlier among the bisector spans near phase 0.0, corresponding to a spectrum taken through considerable clouds, the FAP is reduced to 6.4%, still not very compelling. We examined this further by considering the possibility that the slight apparent changes in the line profiles might be caused by contamination not from an unresolved eclipsing binary, but from scattered moonlight under partly cloudy observing conditions. Evidence of this effect was seen in one of our previous discoveries, HAT-P-12 (Hartman et al. 2009). Following the same procedures used there, we computed the sky contamination factor (SCF) for each of our spectra of HAT-P-14, which quantifies the sky brightness due to moonlight and also accounts for the velocity difference between the moon and the star. We then contrasted the SCF values against the corresponding bisector spans. This is shown in Figure 4. A rather clear trend seems to emerge, suggesting that the distortions in the line shapes as measured by the bisector spans could indeed be due to contamination from moonlight. A Spearman rank-order correlation test excluding the same outlier as before confirms this, giving a FAP of only 0.04%. The apparent correlation between the bisector spans and the velocities in Figure 2 reflects the fact that the six spectra taken during the second half of the

Table 2
High-precision Differential Photometry of HAT-P-14

BJD (2,454,000+)	Δi[a] (mag)	$\sigma_{\Delta i}$ (mag)	Orig. Mag[b] (mag)
759.57643	0.00505	0.00076	8.54130
759.57670	0.00281	0.00076	8.53918
759.57697	0.00561	0.00075	8.54200
759.57725	0.00948	0.00076	8.54627
759.57754	0.00333	0.00075	8.53897

Notes.
[a] The out-of-transit level has been subtracted. These magnitudes have been subjected to the EPD and TFA procedures, carried out simultaneously with the transit fit.
[b] Raw magnitude values without application of the EPD and TFA procedures.
(This table is available in its entirety in a machine-readable form in the online journal. A portion is shown here for guidance regarding its form and content.)

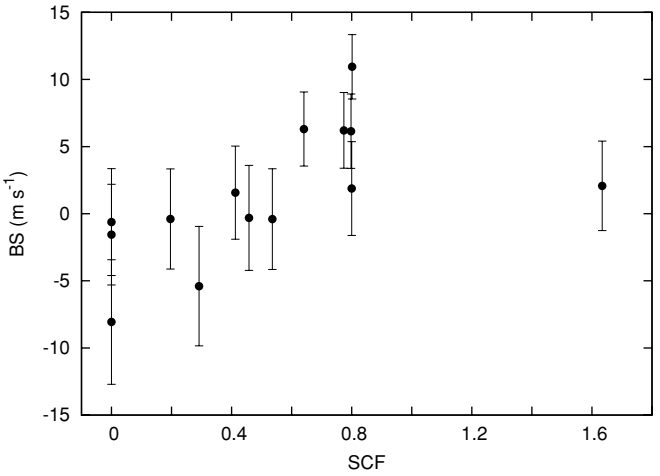

Figure 4. Bisector spans (BS) shown as a function of the sky contamination factor (SCF; see Hartman et al. 2009), which is a measure of the influence of scattered moonlight in each of our spectra (see the text). One outlier has been removed, corresponding to the last Keck/HIRES observation listed in Table 1, which was obtained under cloudy conditions. The correlation is statistically significant, as indicated by a Spearman rank-order correlation FAP of 0.04%.

orbit happen to have SCF values that are larger, on average, than those in the first half. Based on the above, we conclude that the small changes in the line shapes as measured by the highly sensitive bisector spans are well explained by contamination from scattered moonlight, and that there is no real correlation with the RVs. The RV variations in HAT-P-14 are therefore real, and must be due to a planetary companion in orbit around the star.

4. ANALYSIS

4.1. Properties of the Parent Star

Fundamental parameters of the host star HAT-P-14 such as the mass ($M_\star$) and radius ($R_\star$), which are needed to infer the planetary properties, depend strongly on other stellar quantities that can be derived spectroscopically. For this we have relied on our template spectrum obtained with the Keck/HIRES instrument, and the analysis package known as Spectroscopy Made Easy (SME; Valenti & Piskunov 1996), along with the atomic line database of Valenti & Fischer (2005). This analysis yielded the following *initial* values: effective temperature $T_{\rm eff\star} = 6310 \pm 80$ K, surface gravity $\log g_\star = 3.80 \pm 0.10$ (cgs), metallicity [Fe/H] $= -0.02 \pm 0.05$ dex, and projected rotational velocity $v \sin i = 8.8 \pm 0.5$ km s^{-1}. The temperature and metallicity uncertainties have been conservatively increased by a factor of 2 over their nominal values, based on previous experience, to account for possible systematic errors.

In principle, the effective temperature and metallicity, along with the surface gravity taken as a luminosity indicator, could be used as constraints to infer the stellar mass and radius by comparison with stellar evolution models. However, the effect of $\log g_\star$ on the spectral line shapes is rather subtle, and as a result it is typically difficult to determine accurately, so that it is a rather poor luminosity indicator for this particular application. A trigonometric parallax is unfortunately unavailable for HAT-P-14 since the star was not included among the targets of the *Hipparcos* mission (Perryman et al. 1997), despite being bright enough. In any case, for planetary transits a stronger constraint on the luminosity is often provided by $a/R_\star$, the normalized semimajor axis, which is closely related to $\rho_\star$, the mean stellar density. The quantity $a/R_\star$ can be derived directly from the transit light curves (see Sozzetti et al. 2007, and also Section 4.2). This, in turn, allows us to improve on the determination of the spectroscopic parameters by supplying an indirect constraint on the weakly determined spectroscopic value of $\log g_\star$ that removes degeneracies. We take this approach here, as described below.

Our initial values of $T_{\rm eff\star}$, $\log g_\star$, and [Fe/H] were used to determine auxiliary quantities needed in the global modeling of the follow-up photometry and RVs (specifically, the limb-darkening coefficients). This modeling, the details of which are described in the next section, uses a Monte Carlo approach to deliver the numerical probability distribution of $a/R_\star$ and other fitted variables. For further details we refer the reader to Pál (2009b). When combining $a/R_\star$ (used as a proxy for luminosity) with assumed Gaussian distributions for $T_{\rm eff\star}$ and [Fe/H] based on the SME determinations, a comparison with stellar evolution models allows the probability distributions of other stellar properties to be inferred, including $\log g_\star$. Here we use the stellar evolution calculations from the Yonsei-Yale (YY) series by Yi et al. (2001). The comparison against the model isochrones was carried out for each of 10,000 Monte Carlo trial sets (see Section 4.2). Parameter combinations corresponding to unphysical locations in the H-R diagram (1% of the trials) were ignored, and replaced with another randomly drawn parameter set. The result for the surface gravity, $\log g_\star = 4.25 \pm 0.03$, is significantly different from our initial SME analysis, which is not surprising in view of the strong correlations among $T_{\rm eff\star}$, [Fe/H], and $\log g_\star$ that are often present in spectroscopic determinations. Therefore, we carried out a second iteration in which we adopted this value of $\log g_\star$ and held it fixed in a new SME analysis (coupled with a new global modeling of the RV and light curves), adjusting only $T_{\rm eff\star}$, [Fe/H], and $v \sin i$. This gave $T_{\rm eff\star} = 6600 \pm 90$ K, [Fe/H] $= +0.11 \pm 0.08$, and $v \sin i = 8.4 \pm 0.5$ km s^{-1}, in which the conservative uncertainties for the first two have been increased by a factor of 2 over their formal values, as before. A further iteration did not change $\log g_\star$ significantly, so we adopted the values stated above as the final atmospheric properties of the star. They are collected in Table 3, together with the adopted values for the macroturbulent and microturbulent velocities.

We note that the effective temperature also changed rather significantly from the first SME iteration, by about 300 K. An external check on the accuracy of $T_{\rm eff\star}$ may be obtained from color indices derived from existing brightness measurements for HAT-P-14. Photometric measurements on a standard system are available from the Tycho-2, 2MASS, and TASS catalogs (Høg et al. 2000; Skrutskie et al. 2006; Droege et al. 2006), and are summarized in the second block of Table 3. We constructed seven different color indices, and applied color/temperature calibrations by Ramírez & Meléndez (2005; available for six of the color indices), Casagrande et al. (2006; four color indices), and González Hernández & Bonifacio (2009; five color indices). These relations include terms that depend on metallicity. Because such photometric temperatures are very sensitive to reddening, we examined the dust maps by Schlegel et al. (1998) in the direction to HAT-P-14 and obtained $E(B-V) = 0.030$, after a small correction for distance using the value of 205 ± 11 pc reported below. Two other reddening estimates of 0.022 and 0.033 were obtained similarly from Burstein & Heiles (1982) and Hakkila et al. (1997), respectively. We adopt the straight average of the three measures, $E(B-V) = 0.028 \pm 0.015$, with a conservative uncertainty.

Table 3
Stellar Parameters for HAT-P-14

Parameter	Value	Source
	Spectroscopic properties	
$T_{\rm eff\star}$ (K)	6600 ± 90	SME[a]
[Fe/H]	+0.11 ± 0.08	SME
$v \sin i$ (km s^{-1})	8.4 ± 0.5	SME
$v_{\rm mac}$ (km s^{-1})	5.30	SME
$v_{\rm mic}$ (km s^{-1})	0.85	SME
$\gamma_{\rm RV}$ (km s^{-1})	−20.81 ± 0.28	DS
	Photometric properties	
B_T (mag)	10.494 ± 0.031	Tycho-2
V_T (mag)	10.038 ± 0.029	Tycho-2
V (mag)	9.980 ± 0.058	TASS
I_C (mag)	9.453 ± 0.102	TASS
J (mag)	9.094 ± 0.021	2MASS
H (mag)	8.927 ± 0.020	2MASS
K_s (mag)	8.851 ± 0.019	2MASS
$E(B-V)$ (mag)	0.028 ± 0.015	Dust maps[b]
	Derived properties	
$M_\star$ ($M_\odot$)	1.386 ± 0.045	YY+$a/R_\star$+SME[c]
$R_\star$ ($R_\odot$)	1.468 ± 0.054	YY+$a/R_\star$+SME
$\log g_\star$ (cgs)	4.25 ± 0.03	YY+$a/R_\star$+SME
$L_\star$ ($L_\odot$)	3.66 ± 0.37	YY+$a/R_\star$+SME
M_V (mag)	3.31 ± 0.12	YY+$a/R_\star$+SME
Age (Gyr)	1.3 ± 0.4	YY+$a/R_\star$+SME
Distance (pc)	205 ± 11	YY+$a/R_\star$+SME

Notes.
[a] SME: "Spectroscopy Made Easy" package for the analysis of high-resolution spectra (Valenti & Piskunov 1996). These parameters rely primarily on SME, but have a small dependence also on the iterative analysis incorporating the isochrone search and global modeling of the data, as described in the text.
[b] Average of results from Schlegel et al. (1998), Burstein & Heiles (1982), and Hakkila et al. (1997), with small corrections for distance.
[c] YY+$a/R_\star$+SME: based on the YY isochrones (Yi et al. 2001), $a/R_\star$ as a luminosity indicator, and the SME results.

We corrected each of the color indices for reddening, and computed weighted temperature averages for each set of calibrations, with weights determined from the individual temperature uncertainties. The latter include all photometric errors, the uncertainty in both the reddening and the metallicity, and the scatter of the calibrations themselves. The seven color indices are not completely independent, but nevertheless give a useful sense of the scatter. The agreement between the 15 separate estimates from all three calibrations is quite satisfactory, the dispersion being 112 K. The mean of the three calibration averages is $T_{\rm eff} = 6598 \pm 100$ K, which is in excellent accord with the final spectroscopic value from SME and supports its accuracy.

With the adopted spectroscopic parameters the model isochrones yield the stellar mass and radius $M_\star = 1.386 \pm 0.045\ M_\odot$ and $R_\star = 1.468 \pm 0.054\ R_\odot$, along with other properties listed at the bottom of Table 3. HAT-P-14 is a slightly evolved F star with an estimated age of 1.3 ± 0.4 Gyr, according to these models. The inferred location of the star in a diagram of $a/R_\star$ versus $T_{\rm eff\star}$, analogous to the classical H-R diagram, is shown in Figure 5. The stellar properties and their 1σ and 2σ confidence ellipsoids are displayed against the backdrop of Yi et al. (2001) isochrones for the measured metallicity of [Fe/H] = +0.11, and a range of ages. For comparison, the location implied by the initial SME results is also shown (triangle), and corresponds to a somewhat more evolved state.

The distance to the star may be obtained by comparing the absolute magnitudes inferred from the stellar evolution models

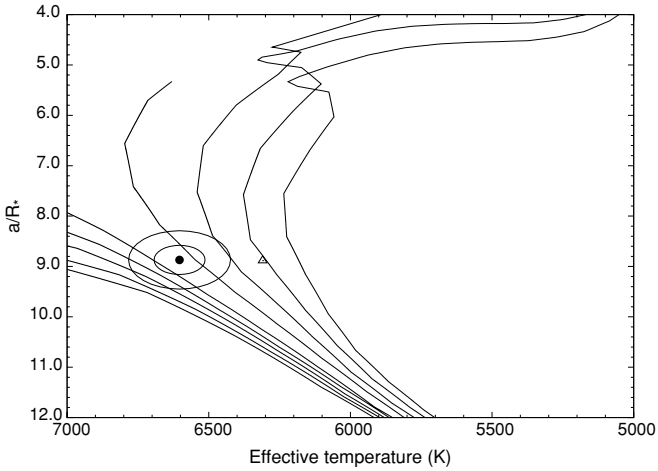

Figure 5. Model isochrones from Yi et al. (2001) for the measured metallicity of HAT-P-14, [Fe/H]= +0.11, and ages of 0.2, 0.4, 0.6, 0.8, 1.0, 1.5, 2.0, 2.5, and 3.0 Gyr (left to right). The adopted values of $T_{\rm eff\star}$ and $a/R_\star$ are shown together with their 1σ and 2σ confidence ellipsoids. The initial values of $T_{\rm eff\star}$ and $a/R_\star$ from the first SME and light curve analyses are represented with a triangle.

against the apparent brightness measurements mentioned earlier. For this we use the V, I_C, J, H, and K_s magnitudes, corrected for extinction using $A(V) = 3.1 \times E(B-V)$ appropriately scaled to each passband following Cardelli et al. (1989). The near-infrared magnitudes from 2MASS were transformed to the ESO system of the isochrones using the relations by Carpenter (2001). The five distance estimates agree with each other to within a few pc. The average is 205 ± 11 pc, where the uncertainty includes all sources of error (photometric and spectroscopic), but excludes possible systematics from the evolution models themselves, which are difficult to quantify.

4.2. Global Modeling of the Data

This section describes the procedure we followed to model the HATNet photometry, the follow-up photometry, and the RVs simultaneously. Our model for the follow-up light curves used analytic formulae from Mandel & Agol (2002) for the eclipse of a star by a planet, with limb darkening being prescribed by a quadratic law. The limb darkening coefficients for the Sloan i band were interpolated from the tables by Claret (2004) for the spectroscopic parameters of the star as determined from the SME analysis (Section 4.1). The transit shape was parametrized by the normalized planetary radius $p \equiv R_p/R_\star$, the square of the impact parameter b^2, and the reciprocal of the half-duration of the transit $\zeta/R_\star$. We chose these parameters because of their simple geometric meanings and the fact that they show negligible correlations (see Bakos et al. 2010). The relation between $\zeta/R_\star$ and the quantity $a/R_\star$, used in Section 4.1, is given by

$$a/R_\star = P/2\pi(\zeta/R_\star)\sqrt{1-b^2}\sqrt{1-e^2}/(1+e\sin\omega) \qquad (1)$$

(see, e.g., Tingley & Sackett 2005). Our model for the HATNet data was the simplified "P1P3" version of the Mandel & Agol (2002) analytic functions (an expansion in terms Legendre polynomials), for the reasons described by Bakos et al. (2010). Following the formalism presented by Pál (2009a), the RVs were fitted with an eccentric Keplerian model parametrized by the semiamplitude K and Lagrangian elements $k \equiv e\cos\omega$ and $h \equiv e\sin\omega$, in which ω is the longitude of periastron.

We assumed that there is a strict periodicity in the individual transit times. We assigned the transit number $N_{\rm tr} = 0$ to the first complete follow-up light curve gathered on 2009 March 25. The adjustable parameters in the fit that determine the ephemeris were chosen to be the time of the first transit center in HATNet field G195, $T_{c,-473}$, and that of the last transit center observed with the FLWO 1.2 m telescope, $T_{c,+11}$. We used these as opposed to the period and reference epoch in order to minimize correlations between parameters (see Pál et al. 2008). Times of mid-transit for intermediate events were interpolated using these two epochs and the corresponding transit number of each event, $N_{\rm tr}$. The eight main parameters describing the physical model were thus $T_{c,-473}$, $T_{c,+11}$, $R_p/R_\star$, b^2, $\zeta/R_\star$, K, $k \equiv e\cos\omega$, and $h \equiv e\sin\omega$. Five additional ones were included that have to do with the instrumental configuration. These are the HATNet blend factors $B_{\rm inst}$ (one for each HATNet field, G194 and G195), which account for possible dilution of the transit in the HATNet light curves from background stars due to the broad PSF (20′ FWHM), the HATNet out-of-transit magnitudes $M_{0,\rm HATNet}$ (one for each field), and the relative zero point $\gamma_{\rm rel}$ of the Keck RVs.

We extended our physical model with an instrumental model that describes brightness variations caused by systematic errors in the measurements. This was done in a similar fashion to the analysis presented by Bakos et al. (2010). The HATNet photometry had already been EPD- and TFA-corrected before the global modeling, so we only considered corrections for systematics in the follow-up light curves. We chose the "ELTG" method, i.e., EPD was performed in "local" mode with EPD coefficients defined for each night, and TFA was performed in "global" mode using the same set of stars and TFA coefficients for all nights. The five EPD parameters were the hour angle (representing a monotonic trend that changes linearly over time), the square of the hour angle (reflecting elevation), and the stellar profile parameters (equivalent to the FWHM, elongation, and position angle of the image). The functional forms of the above effects contained six coefficients, including the auxiliary out-of-transit magnitude of the individual events. The EPD parameters were independent for all five nights, implying 30 additional coefficients in the global fit. For the global TFA analysis we chose 20 template stars that had good quality measurements for all nights and on all frames, implying an additional 20 parameters in the fit. Thus, the total number of fitted parameters was 13 (physical model with 5 configuration-related parameters) + 30 (local EPD) + 20 (global TFA) = 63, i.e., much smaller than the total number of data points (1711).

The joint fit was performed as described in Bakos et al. (2010). We minimized χ^2 in the space of parameters by using a hybrid algorithm, combining the downhill simplex method (AMOEBA; see Press et al. 1992) with a classical least-squares algorithm. Uncertainties for the parameters were derived applying the Markov Chain Monte Carlo method (MCMC; see Ford 2006) using "Hyperplane-CLLS" chains (Bakos et al. 2010). This provided the full a posteriori probability distributions of all adjusted variables. The length of the chains was 10,000 points. The a priori distributions of the parameters for these chains were chosen to be Gaussian, with eigenvalues and eigenvectors derived from the Fisher covariance matrix for the best-fit solution. The Fisher covariance matrix was calculated analytically using the partial derivatives given by Pál (2009a).

5. RESULTS

With the procedure above we obtained the a posteriori distributions for all fitted variables, and other quantities of interest such as $a/R_\star$. As described in Section 4.1, $a/R_\star$ was used together with stellar evolution models to infer a theoretical value for $\log g_\star$ that is significantly more accurate than the spectroscopic value. The improved estimate was in turn applied to a second iteration of the SME analysis, as explained previously, in order to obtain better estimates of $T_{\rm eff\star}$ and [Fe/H]. The global modeling was then repeated with updated limb-darkening coefficients based on those new spectroscopic determinations. The resulting geometric parameters pertaining to the light curves and velocity curves are listed in Table 4.

Table 4
Orbital and Planetary Parameters

Parameter	Value
Light curve parameters	
P (days)	4.627669 ± 0.000005
T_c (BJD)[a]	$2,454,875.28938 \pm 0.00047$
T_{14} (days)[a]	0.0912 ± 0.0017
$T_{12} = T_{34}$ (days)[a]	0.0287 ± 0.0026
$a/R_\star$	8.87 ± 0.29
$\zeta/R_\star$	29.53 ± 0.42
$R_p/R_\star$	0.0805 ± 0.0015
b^2	$0.794^{+0.012}_{-0.014}$
$b \equiv a\cos i/R_\star$	$0.891^{+0.007}_{-0.008}$
i (deg)	83.5 ± 0.3
Limb-darkening coefficients (Sloan i band)[b]	
c_1 (linear term)	0.1089
c_2 (quadratic term)	0.2439
RV parameters	
K (m s^{-1})	219.0 ± 3.3
$k \equiv e\cos\omega$[c]	-0.009 ± 0.009
$h \equiv e\sin\omega$[c]	0.106 ± 0.013
e	0.107 ± 0.013
ω (deg)	94 ± 4
RV jitter (m s^{-1})	7.3
$\sigma_{\rm RV}$ (m s^{-1})	8.1
Planetary parameters	
M_p ($M_{\rm J}$)	2.232 ± 0.059
R_p ($R_{\rm J}$)	1.150 ± 0.052
$C(M_p, R_p)$[d]	0.45
ρ_p (g cm^{-3})	1.82 ± 0.24
$\log g_p$ (cgs)	3.621 ± 0.037
a (AU)	0.0606 ± 0.0007
$T_{\rm eq}$ (K)	1570 ± 34
Θ[e]	0.168 ± 0.008
$\langle F\rangle$ (10^9 erg s^{-1} cm^{-2})[f]	1.37 ± 0.12

Notes.
[a] T_c: reference epoch of mid-transit that minimizes the correlation with the orbital period. It corresponds to $N_{\rm tr} = -9$. T_{14}: total transit duration, i.e., the interval of time between the first and last contacts; $T_{12} = T_{34}$: ingress/egress time, i.e., the time interval between the first and second, or third and fourth contacts.
[b] Values for a quadratic law, adopted from the tabulations by Claret (2004) according to the spectroscopic (SME) parameters listed in Table 3.
[c] Lagrangian orbital parameters derived from the global modeling, and primarily determined by the RV data.
[d] Correlation coefficient between the planetary mass M_p and radius R_p.
[e] Safronov number given by $\Theta = \frac{1}{2}(V_{\rm esc}/V_{\rm orb})^2 = (a/R_p)(M_p/M_\star)$ (see Hansen & Barman 2007).
[f] Incoming flux per unit surface area, averaged over the slightly eccentric orbit.

The rms residual of the RV measurements from the orbital fit is 8.1 m s^{-1}.

Included in this table is the RV "jitter." This is a component of assumed astrophysical noise intrinsic to the star that we added in quadrature to the internal errors for the RVs in order to achieve χ^2/dof = 1 from the RV data for the global fit. Auxiliary parameters not listed in the table are $T_{c,-473}$ = 2,452,728.0512 ± 0.0024 (BJD), $T_{c,+11}$ = 2,454,967.8427 ± 0.0005 (BJD), the blending factors B_{instr} = 0.73 ± 0.09 for HATNet field G194 and B_{instr} = 0.96 ± 0.04 for field G195, and γ_{rel} = 26.6 ± 2.4 m s^{-1}. The latter quantity represents an arbitrary offset for the Keck RVs, and does *not* correspond to the true center of mass velocity of the system, which was listed earlier in Table 3 (γ_{RV}).

The planetary parameters and their uncertainties can be derived by combining the a posteriori distributions for the stellar, light curve, and RV parameters. In this way we find a mass for the planet of M_p = 2.232 ± 0.059 M_J and a radius of R_p = 1.150 ± 0.052 R_J, leading to a mean density ρ_p = 1.82 ± 0.24 g cm^{-3}. These and other planetary parameters are listed at the bottom of Table 4.

We note that the eccentricity of the orbit is significantly different from zero: e = 0.107 ± 0.013. With a longitude of periastron ω = 95° ± 4°, the orientation of the system is such that the orbit is viewed very nearly along the major axis, with periastron on the near side. Furthermore, the eccentricity is large enough that the separation between the star and the planet when the planet is behind is some 23% larger than at transit. This, combined with the relatively low inclination angle, implies that there should be no occultations of HAT-P-14b. Formally, the impact parameter at the occultation is b_{occult} = 1.102 ± 0.030, which is greater than unity at the 3σ confidence level.

Individual times of mid-transit were measured for each of the five events observed with KeplerCam. This was done by holding fixed all model parameters that define the shape of the transit to their final values in Table 4, and adjusting only the time of the center of the event in each series. The results are listed in Table 5, along with their uncertainties and $O - C$ residuals from the ephemeris for the planet. As expected, the events with only partial coverage of the transit (first two in Table 5; see also Figure 3) have larger uncertainties and residuals.

As a final note, the barycentric Julian dates in this table and throughout the paper are calculated from Coordinated Universal Time (UTC), in which a second has the same duration as a second of International Atomic Time (TAI), but the scale is subject to occasional 1 s adjustments (leap seconds) to stay in pace with the slowly and irregularly decreasing rotation rate of the Earth. UTC (the basis of civil time) is therefore not continuous, and is unsuitable as a physical time coordinate. This can be important for some applications that combine timing measurements over long periods of time (e.g., Guinan & Ribas 2001), a problem that has long been recognized in the binary star community (for a pointed discussion, see Bastian 2000) as well as the solar system and pulsar communities. Timing measurements in the transiting planet field now span a decade, and although the differential effect over this period is only a few seconds (significantly smaller than the typical measurement precision), it will become more important in the future. The issue has already been mentioned recently in the context of studying transit timing variations (TTVs) for transiting planets (Adams et al. 2010). While the use of Terrestrial Time (TT = TAI + 32.184 seconds) as the basis for Julian date calculations eliminates the problem, for practical reasons virtually all the JDs (and BJDs) reported in previous transiting planet studies, including those in the HATNet series, are implicitly on the UTC scale. We continue this practice here, but caution the reader that the TT−UTC corrections need to be taken into account for the most demanding applications.

Table 5
Transit Timing Measurements for HAT-P-14

N_{tr}	T_c (BJD−2,454,000)	σ_{T_c} (days)	$O - C$ (s)
−34	759.59280	0.00290	−458
−11	866.03268	0.00273	−127
+0	916.93940	0.00081	+90
+3	930.82160	0.00114	+24
+11	967.84186	0.00088	−59

6. DISCUSSION

At V = 9.98, HAT-P-14 is among the brightest TEP host stars presently known (only 11 of the other 66 are brighter), which should facilitate a wide range of follow-up studies. Our planetary mass determination of M_p = 2.23 M_J places HAT-P-14b in the category of the massive transiting planets discovered to date, which seem to be less common than those with smaller masses. In fact, a look at the mass distribution for the known transiting systems shows that it falls off precisely around 2 M_J. Since there is no obvious selection effect that would make these massive objects more difficult to detect or confirm (such as smaller radii, longer orbital periods, or fainter or hotter parent stars), it may be that they are indeed less common as a population. It has also been noticed (e.g., Southworth et al. 2009; Joshi et al. 2009) that the most eccentric cases among the transiting planets are all massive: all systems with $e > 0.2$ are more massive than 3 M_J, although the numbers are still small. A similar trend is seen among the non-transiting planets, bearing in mind the sin i ambiguity in their masses. Among the transiting systems whose spin-orbit alignment has been measured through observation of the Rossiter–McLaughlin effect, it would also appear that the more massive ones are disproportionately misaligned compared to the ones with smaller-mass planets, considering their relative populations, although again the numbers are as yet too small to be conclusive. Obviously it would be useful to determine the spin-orbit alignment of the HAT-P-14 system, which should be readily measurable given that $v \sin i$ = 8.4 km s^{-1}.

The mass of HAT-P-14b is quite similar to the recently discovered Kepler-5b (Koch et al. 2010), but its radius is about 20% smaller. A comparison with the evolution models of Fortney et al. (2007), at an equivalent solar semimajor axis of a_{equiv} = 0.0317 AU, indicates that the radius of HAT-P-14b is well reproduced for the 1.3 Gyr age of the system if it has about 50 $M_\oplus$ worth of heavy elements in its interior (about 7% of its total mass). This amount of metals is consistent with the correlation between core mass and metallicity of the parent star proposed by Guillot et al. (2006) and Burrows et al. (2007), which seems to support the core-accretion mode of planet formation. The incident flux we compute for the planet averaged over its eccentric orbit, $\langle F \rangle$ = (1.37 ± 0.12) × 10^9 erg s^{-1} cm^{-2}, places it in the proposed pM category of Fortney et al. (2008). These objects are expected to present temperature inversions in their atmospheres, and large day/night temperature contrasts. The equilibrium temperature of HAT-P-14b, assuming zero albedo and full redistribution of the incident radiation, is 1570 ± 34 K.

The non-zero eccentricity of the orbit for the relatively short period of 4.6 days raises the question of whether tidal forces have had enough time to circularize the orbit at the 1.3 ± 0.4 Gyr age of the system, or alternatively, whether there might be a second planet perturbing the orbit of HAT-P-14b and pumping up its eccentricity. Following Adams & Laughlin (2006), we estimate the timescale for tidal circularization to be $\tau_{\rm circ} \approx 0.33$ Gyr, although this is a strong function of the poorly known tidal quality factor Q_p, for which we have adopted here the commonly used value of 10^5. For $Q_p \simeq 10^6$ the timescale is 10 times longer, and a recent study of the 0.78-day transiting planet WASP-19b has suggested Q_p could be much larger still (Hebb et al. 2010). Consequently we cannot rule out that the eccentricity we measure for HAT-P-14b is primordial, at least in part, nor can we exclude the presence of a second planet in the system.

The grazing orientation ($b = 0.891^{+0.007}_{-0.008}$) significantly enhances the detection sensitivity to additional planets in the system. These could manifest themselves through transit *duration* variations (TDVs), or equivalently, changes in the orbital inclination angle as has been claimed for TrES-2b by Mislis & Schmitt (2009) and Mislis et al. (2010), and recently disputed by Scuderi et al. (2010). Perturbing planets may also induce variations in the times of mid-transit (transit *timing* variations, or TTVs) through gravitational interaction (e.g., Dobrovolskis & Borucki 1996; Holman & Murray 2005). In general, there exists no exact closed-form expressions for evaluating the amplitudes of such signals since no general solution to the three-body problem exists. One typical approach is to employ an approximation to simplify the problem. Agol et al. (2005) provided useful analytic expressions for the case of a coplanar system where the host star has a much larger mass than the two companion planets, for several different scenarios. The largest TTVs occur for planets in mean motion resonance, and we may use expressions (33) and (34) from Agol et al. (2005) to estimate the amplitude and libration period of the TTV signal in a 2:1 resonance. For the HAT-P-14 system we find that such a planet would induce a peak-to-peak deviation in the timings of 13.6 s and 126.3 s for a mass of 0.1 $M_\oplus$ and 1 $M_\oplus$, respectively, and the libration period would be ∼175 days. Thus, an Earth-mass planet in this configuration would be eminently detectable with further observations. Out-of-resonance perturbers can be considered using Equation (32) of Agol et al. (2005), but we find they lead to sub-second amplitudes for various configurations, far beyond the current measurement capabilities.

The properties of HAT-P-14b also make it attractive for a future search for a companion satellite ("exomoon"). The Hill radius (R_H) extends to 8.1 planetary radii (9.1 R_J), and using the expressions of Domingos et al. (2006), which account for the planet's orbital eccentricity, the maximum distance at which an exomoon could be stable for this planet would be $0.436\,R_H$ and $0.824\,R_H$ for a prograde and retrograde exomoon, respectively. Barnes & O'Brien (2002) presented analytic approximations for the maximum stable exomoon mass for close-in extrasolar giant planets based upon tidal dissipation arguments, which were shown to provide excellent agreement with numerical integrations. Assuming again a tidal dissipation value of $Q_p \simeq 10^5$ and a Love number of $k_{2p} \simeq 0.51$, the maximum stable moon mass over the 1.3 Gyr lifetime of the star is $0.002\,M_\oplus$ and $0.12\,M_\oplus$ for a moon at the maximum planet–moon separations for prograde and retrograde orbits, respectively. For $Q_p \simeq 10^6$ these limits would be 10 times larger, or $1.2\,M_\oplus$ in the retrograde case. Such exomoons would produce small TTVs, but the highly grazing orientation provides a better means of detection. Kipping (2009a, 2009b) showed that an exomoon induces two types of transit duration variations on the host planet: a sky-projected tangential velocity variation (the V-component), and a spatially orthogonal transit impact parameter variation (the TIP component). While the TTV and TDV-V rms amplitudes of a 1.2 $M_\oplus$ exomoon would be 4.5 s and 1.0 s, respectively, the TDV-TIP component could be as high as 16 s or 45 s peak-to-peak for the optimum configuration of a favorably inclined exomoon. For comparison, another near-grazing transiting planet is TrES-2b (O'Donovan et al. 2006), and repeating the same calculation (with $Q_p \simeq 10^6$, as above) we find that the maximal TDV-TIP of the maximum-mass stable retrograde exomoon would be only 0.07 s. The much smaller value in this case is mostly due to the low maximum stable moon mass of 0.005 $M_\oplus$, as a result of the lower planetary mass and longer system age. We suggest, therefore, that future monitoring of the transit duration of HAT-P-14b could allow for interesting constraints not only on the presence of additional planets, but also of sub-Earth mass or Earth mass exomoons.

HATNet operations have been funded by NASA grants NNG04GN74G and NNX08AF23G, and SAO IR&D grants. G.T. acknowledges partial support from NASA grant NNX09AF59G. G.Á.B. and J.A.J. were supported by Postdoctoral Fellowships of the NSF Astronomy and Astrophysics Program (AST-0702843 and AST-0702821, respectively). We acknowledge partial support also from the *Kepler* Mission under NASA Cooperative Agreement NCC2-1390 (D.W.L., PI). G.K. thanks the Hungarian Scientific Research Foundation (OTKA) for support through grant K-81373. G.Á.B. thanks Gábor Kovács for his help in system management of the HATNet computers while the data analysis was carried out. We are grateful to the anonymous referee for helpful suggestions. This research has benefited from Keck telescope time allocations granted through NOAO (programs A264Hr, A146Hr) and NASA (N049Hr, N018Hr). This research has also made use of the SIMBAD database and the VizieR catalogue access tool, both operated at CDS, Strasbourg, France, of NASA's Astrophysics Data System Abstract Service, and of data products from the Two Micron All Sky Survey (2MASS), which is a joint project of the University of Massachusetts and the Infrared Processing and Analysis Center/California Institute of Technology, funded by NASA and the NSF.

REFERENCES

Adams, F. C., & Laughlin, G. 2006, ApJ, 649, 1004
Adams, E. R., López-Morales, M., Elliot, J. L., Seager, S., & Osip, D. J. 2010, ApJ, 714, 13
Agol, E., Steffen, J., Sari, R., & Clarkson, W. 2005, MNRAS, 359, 567
Baglin, A., et al. 2006, in Proc. The CoRoT Mission Pre-Launch Status—Stellar Seismology and Planet Finding, ed. M. Fridlund et al. (ESA SP-1306; Noordwijk: ESA), 33
Bakos, G. Á., Noyes, R. W., Kovács, G., Stanek, K. Z., Sasselov, D. D., & Domsa, I. 2004, PASP, 116, 266
Bakos, G. Á., et al. 2007, ApJ, 670, 826
Bakos, G. Á., et al. 2010, ApJ, 710, 1724
Barnes, J. W., & O'Brien, D. P. 2002, ApJ, 575, 1087
Bastian, U. 2000, IBVS, 4822, 1
Borucki, W. J., et al. 2010, Science, 327, 977
Burrows, A., Hubeny, I., Budaj, J., & Hubbard, W. B. 2007, ApJ, 661, 502
Burstein, D., & Heiles, C. 1982, AJ, 87, 1165
Butler, R. P., et al. 1996, PASP, 108, 500
Cardelli, J. A., Clayton, G. C., & Mathis, J. S. 1989, ApJ, 345, 245
Carpenter, J. M. 2001, AJ, 121, 2851
Casagrande, L., Portinari, L., & Flynn, C. 2006, MNRAS, 373, 13
Claret, A. 2004, A&A, 428, 1001

Dobrovolskis, A. R., & Borucki, W. J. 1996, BAAS, 28, 1112
Domingos, R. C., Winter, O. C., & Yokoyama, T. 2006, MNRAS, 373, 1227
Droege, T. F., Richmond, M. W., & Sallman, M. 2006, PASP, 118, 1666
Ford, E. 2006, ApJ, 642, 505
Fortney, J. J., Lodders, K., Marley, M. S., & Freedman, R. S. 2008, ApJ, 678, 1419
Fortney, J. J., Marley, M. S., & Barnes, J. W. 2007, ApJ, 659, 1661
González Hernández, J. I., & Bonifacio, P. 2009, A&A, 497, 497
Guillot, T., Santos, N. C., Pont, F., Iro, N., Melo, C., & Ribas, I. 2006, A&A, 453, L21
Guinan, E. F., & Ribas, I. 2001, ApJ, 546, L43
Hakkila, J., Myers, J. M., Stidham, B. J., & Hartmann, D. H. 1997, AJ, 114, 2043
Hansen, B. M. S., & Barman, T. 2007, ApJ, 671, 861
Hartman, J. D., et al. 2009, ApJ, 706, 785
Hebb, L., et al. 2010, ApJ, 708, 224
Høg, E., et al. 2000, A&A, 355, L27
Holman, M. J., & Murray, N. W. 2005, Science, 307, 1288
Joshi, Y. C., et al. 2009, MNRAS, 392, 1532
Kipping, D. M. 2009a, MNRAS, 392, 181
Kipping, D. M. 2009b, MNRAS, 396, 1797
Koch, D. G., et al. 2010, ApJ, 713, L131
Kovács, G., Bakos, G. Á., & Noyes, R. W. 2005, MNRAS, 356, 557
Kovács, G., Zucker, S., & Mazeh, T. 2002, A&A, 391, 369
Latham, D. W. 1992, in ASP Conf. Ser. 32, IAU Coll. 135, Complementary Approaches to Double and Multiple Star Research, ed. H. A. McAlister & W. I. Hartkopf (San Francisco, CA: ASP), 110
Mandel, K., & Agol, E. 2002, ApJ, 580, L171
Marcy, G. W., & Butler, R. P. 1992, PASP, 104, 270
Mislis, D., & Schmitt, J. H. M. M. 2009, A&A, 500, L45
Mislis, D., Schröter, S., Schmitt, J. H. M. M., Cordes, O., & Reif, K. 2010, A&A, 510, 107
O'Donovan, F. T., et al. 2006, ApJ, 651, L61
Pál, A. 2009a, MNRAS, 396, 1737
Pál, A. 2009b, Ph.D. thesis, Eötvös Loránd Univ., Hungary
Pál, A., & Bakos, G. Á. 2006, PASP, 118, 1474
Pál, A., et al. 2008, ApJ, 680, 1450
Perryman, M. A. C., et al. 1997, A&A, 323, L49
Press, W. H., Teukolsky, S. A., Vetterling, W. T., & Flannery, B. P. 1992, Numerical Recipes in C: the Art of Scientific Computing (2nd ed., Cambridge: Cambridge Univ. Press)
Ramírez, I., & Meléndez, J. 2005, ApJ, 626, 465
Schlegel, D., Finkbeiner, D. P., & Davis, M. 1998, ApJ, 500, 525
Scuderi, L. J., Dittmann, J. A., Males, J. R., Green, E. M., & Close, L. M. 2010, ApJ, 714, 462
Skrutskie, M. F., et al. 2006, AJ, 131, 1163
Southworth, J., et al. 2009, ApJ, 707, 167
Sozzetti, A., et al. 2007, ApJ, 664, 1190
Tingley, B., & Sackett, P. D. 2005, ApJ, 627, 1011
Torres, G., Neuhäuser, R., & Guenther, E. W. 2002, AJ, 123, 701
Torres, G., et al. 2007, ApJ, 666, 121
Valenti, J. A., & Fischer, D. A. 2005, ApJS, 159, 141
Valenti, J. A., & Piskunov, N. 1996, A&AS, 118, 595
Vaughan, A. H., Preston, G. W., & Wilson, O. C. 1978, PASP, 90, 267
Vogt, S. S., et al. 1994, Proc. SPIE, 2198, 362
Yi, S. K., et al. 2001, ApJS, 136, 417